Journal of Geophysical Research: Atmospheres

RESEARCH ARTICLE
10.1029/2018JD029059

Special Section:
Bridging Weather and Climate: Subseasonal-to-Seasonal (S2S) Prediction

Skillful Subseasonal Forecasts of Weekly Tornado and Hail Activity Using the Madden-Julian Oscillation

Cory F. Baggett[1], Kyle M. Nardi[1], Samuel J. Childs[1], Samantha N. Zito[2], Elizabeth A. Barnes[1], and Eric D. Maloney[1]

[1]Department of Atmospheric Science, Colorado State University, Fort Collins, CO, USA, [2]School of Marine and Atmospheric Sciences, Stony Brook University, Stony Brook, NY, USA

Abstract In the United States, severe weather poses a threat to society, producing tornadoes and hail that can result in hundreds of casualties and billions of dollars in damages. Fortunately, skillful predictions of severe weather for short lead times of 0–8 days and longer lead times exceeding 1 month have been realized. However, this leaves a *forecast gap* at subseasonal to seasonal lead times of 2–5 weeks, when early-action decision making by stakeholders is typically made. Here we develop an empirical prediction model that fills this gap during March–June when severe weather is most prevalent across the United States. We demonstrate skillful weekly forecasts of opportunity with lead times of 2–5 weeks of environmental parameters favorable to severe weather, as well as actual tornado and hail activity. To attain this skill, we use as a predictor the current state of active phases of the Madden-Julian Oscillation, known to have physical teleconnections with future weather over the United States. The model has significant skill in regions such as the Plains and the Southeast, providing stakeholders with valuable extended forewarning.

Plain Language Summary In the United States, severe thunderstorms produce tornadoes and large hail, responsible for hundreds of deaths and injuries and many billions of dollars in damages on average each year. Because of these devastating impacts, there is a keen interest to accurately forecast when and where severe thunderstorms are likely to occur. While meteorologists and computer models do reasonably well in forecasting severe thunderstorm activity up to a week in advance, their forecasts are less reliable in the 2- to 5-week time frame. In our study, we develop a technique that can accurately forecast severe thunderstorm activity in this time frame by using knowledge of the current state of weather in the tropics. These accurate, extended forecasts offer valuable forewarning to both the general public and stakeholders of when and where potentially deadly severe thunderstorm activity is likely to occur.

Key Points:
- An active Madden-Julian Oscillation (MJO) modulates springtime tornado and hail activity over the next 2–5 weeks across the United States
- Using the MJO as a predictor, skillful weekly forecasts of severe weather with lead times of 2–5 weeks can be realized
- These subseasonal to seasonal (S2S) forecasts offer important forewarning to stakeholders of when and where severe weather is likely

Supporting Information:
- Supporting Information S1

Correspondence to:
C. F. Baggett,
cbaggett@rams.colostate.edu

Citation:
Baggett, C. F., Nardi, K. M., Childs, S. J., Zito, S. N., Barnes, E. A., & Maloney, E. D. (2018). Skillful subseasonal forecasts of weekly tornado and hail activity using the Madden-Julian Oscillation. *Journal of Geophysical Research: Atmospheres*, *123*, 12,661–12,675. https://doi.org/10.1029/2018JD029059

Received 24 MAY 2018
Accepted 3 NOV 2018
Accepted article online 12 NOV 2018
Published online 26 NOV 2018

Author Contributions:
Conceptualization: Cory F. Baggett, Kyle M. Nardi, Samuel J. Childs, Elizabeth A. Barnes, Eric D. Maloney
Data curation: Cory F. Baggett, Kyle M. Nardi, Samuel J. Childs
Formal analysis: Cory F. Baggett, Kyle M. Nardi, Samuel J. Childs, Samantha N. Zito
Funding acquisition: Elizabeth A. Barnes, Eric D. Maloney
Investigation: Cory F. Baggett, Kyle M. Nardi, Samuel J. Childs, Samantha N. Zito
(continued)

1. Introduction

In the United States, severe convective storms, namely, tornadoes, large hail (>25.4 mm [1 inch]), and high winds (>25.9 m/s [58 mph]), wreak devastation on life and property—resulting in over 900 fatalities and $125 billion in damages over the 2007–2016 period alone (National Oceanic and Atmospheric Administration [NOAA] National Centers for Environmental Information [NCEI], 2018; NOAA Storm Prediction Center [SPC], 2018). During this 10-year period, severe weather was responsible for 54 billion-dollar events, more than all other natural hazards combined (e.g., flooding, droughts, and tropical cyclones; NOAA/NCEI, 2018; Smith & Matthews, 2015). Nine of these 54 events occurred during 2011, including a pair of infamous, multiday events in late April and late May that collectively killed 498 people and caused $21.6 billion in damages (NOAA/NCEI, 2018)—leaving Tuscaloosa, AL, and Joplin, MO devastated in their wake.

Because of these impacts, society and stakeholders have a keen interest in skillful forecasts of when and where severe weather will occur (Allen et al., 2016; Gunturi & Tippett, 2017; NOAA/NCEI, 2018; Simmons & Sutter, 2011; Smith & Matthews, 2015). Fortunately, tremendous progress has been made in understanding the favorable, large-scale environmental conditions that promote the growth, organization, and maintenance of severe thunderstorms—namely, instability, vertical shear, and convective initiation mechanisms (Allen et al., 2015a; Brooks et al., 2003; Gensini & Ashley, 2011; Tippett et al., 2012, 2014, 2015). Forecasts for these favorable environmental conditions are being issued and developed for a variety of time scales at different forecast lead times. For example, the National Oceanic and Atmospheric Administration's Storm Prediction Center (NOAA/SPC) regularly issues skillful probabilistic, daily convective outlooks (Herman et al., 2017) with forecast lead times of 0–3 days and has recently begun issuing 4- to 8-day

Methodology: Cory F. Baggett, Kyle M. Nardi, Samuel J. Childs, Samantha N. Zito, Elizabeth A. Barnes, Eric D. Maloney
Resources: Cory F. Baggett, Kyle M. Nardi, Samuel J. Childs, Elizabeth A. Barnes, Eric D. Maloney
Supervision: Cory F. Baggett, Kyle M. Nardi, Elizabeth A. Barnes, Eric D. Maloney
Validation: Cory F. Baggett, Kyle M. Nardi, Samuel J. Childs, Samantha N. Zito
Visualization: Cory F. Baggett
Writing - original draft: Cory F. Baggett
Writing – review & editing: Cory F. Baggett, Kyle M. Nardi, Samuel J. Childs, Samantha N. Zito, Elizabeth A. Barnes, Eric D. Maloney

outlooks (available at http://www.spc.noaa.gov/products/outlook/). For seasonal outlooks with lead times exceeding 1 month, the El Niño/Southern Oscillation (ENSO) has been shown to influence tornado and hail frequencies in the United States (Allen et al., 2015b; Childs et al., 2018; Cook et al., 2017; Lepore et al., 2017). Skillful seasonal forecasts using ENSO have been demonstrated (Allen et al., 2015b; Lepore et al., 2017) and are of interest to stakeholders (Gunturi & Tippett, 2017).

For intermediate forecast lead times of 2–5 weeks (during the subseasonal portion of the so-called subseasonal to seasonal time scale), skillful guidance for severe weather activity on weekly timescales is currently in its infancy (Allen et al., 2016; Barrett & Gensini, 2013; Barrett & Henley, 2015; Gensini & Allen, 2018; Gensini & Marinaro, 2016; Thompson & Roundy, 2013). While subseasonal forecasts of severe weather have the potential to increase public awareness and preparedness, they could also be beneficial to stakeholders such as emergency managers, catastrophe modelers, and insurance/reinsurance companies (Allen et al., 2016; Gunturi & Tippett, 2017; NOAA/NCEI, 2018; Simmons & Sutter, 2011; Smith & Matthews, 2015). The degree to which subseasonal forecasts could benefit stakeholders was a topic of discussion during the Severe Convection and Climate Workshop held in New York in 2016 (Allen et al., 2016). Unsurprisingly, it was concluded that the utility of skillful subseasonal forecasts to the insurance sector would be largely dependent on both their accuracy and having sufficient lead time to impact business decisions involving risk management. For example, if skillful subseasonal forecasts existed, reinsurers would be better equipped to manage the risk of several high-loss severe thunderstorm events occurring in a single season (e.g., the active 2011 season) in order to maintain adequate coverage for local insurers and their policyholders. It was also concluded that the scientific understanding of the principal drivers of subseasonal variability could be incorporated by catastrophe modelers and thereby assist insurance companies with their decision making (Allen et al., 2016).

Fortunately, to fill the subseasonal *forecast gap*, prior work has identified sources of predictability that have the potential to improve forecasts of severe weather activity in the United States at subseasonal lead times. Two such promising sources of predictability are the Global Wind Oscillation (Gensini & Allen, 2018; Gensini & Marinaro, 2016; Moore, 2017) and the Madden-Julian Oscillation (MJO; Baggett et al., 2017; Barrett & Gensini, 2013; Barrett & Henley, 2015; Kiladis et al., 2014; Matthews, 2008; Mundhenk et al., 2018; Thompson & Roundy, 2013; Wheeler & Hendon, 2004). In this study, we focus on the MJO, which manifests itself in the form of anomalous tropical convection that propagates around the equator with a period of ~30–60 days (Matthews, 2008). Characterized by its amplitude and phase number (1 through 8; Kiladis et al., 2014; Wheeler & Hendon, 2004), the MJO is capable of producing Rossby waves that propagate downstream in time and space, thereby influencing the weather at distant extratropical locations over the following several weeks (Baggett et al., 2017; Henderson et al., 2016; Matthews, 2008; Mundhenk et al., 2018; Sardeshmukh & Hoskins, 1988; Zhang, 2013). Prior work that has examined the relationship between the MJO and severe weather activity has primarily focused on their contemporaneous, statistical relationship. In other words, previous studies have found that the *current* state of the MJO (its amplitude and phase) has a strong association with the *current* state of severe weather activity over the United States (Barrett & Gensini, 2013; Barrett & Henley, 2015; Thompson & Roundy, 2013). For example, Thompson and Roundy (2013) showed that violent tornado days, that is, 24-hr periods with at least six tornadoes rated EF2 or greater on the Enhanced Fujita (EF) scale (McDonald & Mehta, 2006), are more frequent when the MJO is in phase 2 than in phase 8.

In this study, we build on the foundation of these prior works by hypothesizing that the *current* state of the MJO is a source of predictability and predictive skill for *future* severe weather activity over the United States. To test this hypothesis, we composite environmental parameters associated with severe weather activity, along with tornado and hail events themselves, by MJO phase and lead time (i.e., positive lags) to show that these severe weather phenomena are modulated on weekly timescales by the MJO for several weeks following active MJO phases. Furthermore, we construct a simple empirical prediction model to demonstrate that skillful weekly forecasts of severe weather activity can be made with lead times of 2–5 weeks, using only the current state of the MJO as a predictor.

2. Data and Methods

2.1. Environmental Parameters

We derive daily, environmental parameters of surface-based convective available potential energy (CAPE; J/kg), 0- to 3-km storm relative helicity (SRH; m^2/s^2), and their weighted product (CSRH2 = CAPE × SRH^2;

m^6/s^6; Lu et al., 2015; Tippett et al., 2012, 2014) from data acquired from the European Centre for Medium-Range Weather Forecasts (ECMWF) interim reanalysis (ERA-Interim; Dee et al., 2011). The data have a horizontal resolution of 1.5° × 1.5° and span the years 1979–2015. Daily values of afternoon-averaged CAPE are computed by directly downloading from ERA-Interim, and then averaging, the 6-, 9-, and 12-hr forecasts from the 1200 UTC reanalysis (i.e., instantaneous 1800, 2100, and 0000 UTC values). Using afternoon-averaged values of CAPE benefits our analysis because it makes it more likely to capture enhanced values of CAPE should they exist on any given afternoon at any given location. Also, while reanalysis-derived CAPE is a forecast product and therefore subject to forecast errors, it has long been shown to be an adequate discriminator of severe thunderstorm environments (e.g., Brooks et al., 2003). Daily values of afternoon-averaged SRH are computed using the Sounding and Hodograph Analysis and Research Program in Python (SHARPpy), which uses the Bunkers' internal dynamics method to calculate the storm-motion vector (Blumberg et al., 2017; Bunkers et al., 2000). As input, SHARPpy is provided 1800 and 0000 UTC values of the three-dimensional fields of zonal wind and geopotential from ERA-Interim, along with terrain height. From these values it calculates SRH at the aforementioned synoptic time steps, from which afternoon-averaged values are derived. Daily values of CSRH2 are simply found by multiplying the daily, afternoon-averaged values of CAPE by the square of daily, afternoon-averaged values of SRH. The squaring of SRH is based on Eq. 3 of Tippett et al. (2012) where the best Poisson regression fit between monthly tornado occurrence and environmental parameters across the United States includes an SRH coefficient close to 2.

2.2. Tornado and Hail Events

We obtain daily tornado and hail reports data from the SPC's Severe Weather Database (Schaefer & Edwards, 1999). Daily reports of tornadoes with intensities greater than EF1 and hail with diameters greater than 25.4 mm (1 inch) are each aggregated into 1.5° × 1.5° grid boxes, centered on ERA-Interim grid points. We consider a single tornado *event* to have occurred in a given grid box on a particular day if one or more tornado reports occurred therein. In this study, we focus our analysis on regions that subsume 5 × 5 grid boxes (7.5° × 7.5°). Thus, by construction, a region can experience between 0 and 25 tornado events each day. Similarly, a region can experience 0 and 25 hail events each day. In Text S1, we discuss the sensitivity of our results to the well-documented, nonmeteorological heterogeneities that exist in the storm reports data (e.g., Agee & Childs, 2014; Allen & Tippett, 2015).

2.3. The MJO

The MJO dominates intraseasonal variability in the tropics, manifesting itself as tropical convective and zonal wind anomalies that propagate eastward along the equator with a period of ~30–60 days (Kiladis et al., 2014; Wheeler & Hendon, 2004; Zhang, 2013). Several indices have been developed to describe the current state of the MJO, such as the Real-time Multivariate MJO Index (RMM; Wheeler & Hendon, 2004) and the outgoing longwave radiation (OLR)-based MJO Index (OMI; Kiladis et al., 2014). In this study, we use the OMI and show through supporting figures that our results are generally insensitive to the choice of index. As detailed in Kiladis et al. (2014), the daily, principal component time series (PC1 and PC2) of the OMI are calculated by projecting the 20- to 96-day band-passed-filtered, tropical OLR onto the two leading empirical orthogonal functions of the 30- to 96-day eastward band-passed-filtered, tropical OLR. The MJO is typically characterized by one of eight phases, indicative of where tropical convection is active along the equator, and its amplitude, $\sqrt{(PC1^2 + PC2^2)}$. To maintain geographical consistency with the RMM index, we rotate the OMI by multiplying its PC1 by -1 and reverse the order of PC1 and PC2.

2.4. Composite Analysis

Daily anomalies of CAPE, SRH, CSRH2, tornado events, and hail events are found by subtracting from each variable its smoothed, seasonal cycle. The smoothed, seasonal cycle is found by using Fourier analysis to decompose a given variable's raw, calendar-day climatology into its mean and harmonics. Then, the mean and first two harmonics are summed to construct the smoothed, seasonal cycle. The use of two harmonics captures the secondary peak in severe weather activity that typically occurs during the fall, particularly in the Southeast (e.g., Childs et al., 2018). The composites are constructed by selecting days when the MJO's amplitude is $\geq$1 during March–June (MAMJ). For each MJO phase, forward lag composites of consecutive, overlapping weeks (e.g., days +1 through +7 and days +2 through +8) are made for weekly averaged values of anomalous CAPE, SRH, and CSRH2 and for weekly summed values of anomalous tornado and hail events

for their respective 7.5° × 7.5° regions. In keeping with forecasting parlance, we refer to the forward lag dimension of these composites as *lead time*.

2.5. The Empirical Prediction Model, Its Verification, and Its Skill

Following the methods of (Mundhenk et al., 2018), we create a two-class empirical prediction model to forecast weekly values of either above or below normal CAPE, SRH, CSRH2, tornado events, and hail events at subseasonal lead times for the 7.5° × 7.5° regions described in sections 2.2 and 2.4. The model incorporates the initial state of the MJO (according to the OMI) as its only predictor. Forecasts are only initialized on days in MAMJ when the OMI's amplitude is ≥1 (~61% of all MAMJ days). To generate a forecast, the model compares the median of a variable's conditional distribution (that varies by the initialization date's MJO phase and forecast lead time) to the median of its climatological distribution (that varies only by forecast lead time). Depending on whether the variable's conditional distribution's median is greater than or less than the median of its corresponding climatological distribution, the model predicts above or below normal values of the variable, respectively. We choose to define normal using the median rather than the mean due to the skewness of the distributions associated with tornado and hail events. The distributions are created by drawing samples from the daily anomaly time series of each variable that have been, as in the composites, computed over 7.5° × 7.5° regions and over consecutive, overlapping weeks (i.e., a 7-day forward running mean). The relevant climatological distribution for a forecast lead time of 1 week is drawn from 1 March through 30 June; for a lead time of 2 weeks, it is drawn from 8 March through 7 July. Unlike Mundhenk et al. (2018), we allow the climatological distribution to shift as a function of lead time because of the underlying strong seasonality of the anomalies for each variable.

Forecasts for each season are verified independently in a typical leave-one-year-out, cross-validation approach (Johnson et al., 2014; Mundhenk et al., 2018). For example, if the model is forecasting for 2015, then the training data to create the forecast derives from 1979 to 2014 only—meaning all anomalies, their distributions, and their resulting medians are created independently from 2015, the left-out-year. This procedure is repeated 37 times, for each left-out-year. A forecast is verified correct if the observed anomaly in the left-out-year matches the training data's forecasted anomaly; otherwise, the forecast verifies as incorrect.

The verification statistics of this two-class empirical prediction model can be segregated into a typical 2 × 2 contingency table, which we evaluate using the Heidke skill score (HSS; Johnson et al., 2014; Mundhenk et al., 2018; Wilks, 2006). The HSS facilitates a comparison of the empirical prediction model's skill to that of a climatological reference forecast. Formulated, $HSS = 100 \times (H - E)(T - E)^{-1}$, where H equals the number of correct forecasts, E is the number of correct forecasts expected by chance, and T is the total number of forecasts made. Because the model makes a forecast of above or below normal values with respect to the median of a climatological distribution of that value, it is expected, by chance, to be correct $E = T/2$ times (50% of the time). A prediction model that makes correct forecasts all of the time will have an HSS of 100, while one that makes correct forecasts twice as often as incorrect forecasts will have an HSS of 33. A model that makes forecasts with no skill compared to a random forecast receives an HSS of 0, while a model that makes incorrect forecasts more frequently will have a negative HSS.

2.6. Statistical Significance

Results from the empirical prediction model, and their statistical significance, are presented in section 5. The null hypothesis we seek to reject in these results can be stated as, "There is no relationship between current, active MJO phases and forecast skill of severe weather variables at extended lead times." We reject this null hypothesis for certain combinations of MJO phase and lead time through comparing the observed forecast skill to the distribution of skills derived from 1,000 random forecast samples. These random forecast samples are generated via a bootstrapping method, with replacement, from the original data. Because the MJO often resides in a particular phase during *blocks* of several days in a row (see Table S1), there is autocorrelation imbedded in the observed forecast that must be reproduced in the random forecast samples. Thus, to reproduce this autocorrelation, we randomize the blocks of days that the MJO is observed to be active. To accomplish this, each of the 566 blocks (sum of the third column in Table S1a) is assigned a random date for the first day of the block (from all MAMJ days during 1979–2015). Then each block is assigned a random MJO phase (1 through 8). Having randomized the MJO blocks, the empirical prediction model (as described in section 2.5) is then run, using the randomized MJO blocks on the original data to create a unique random

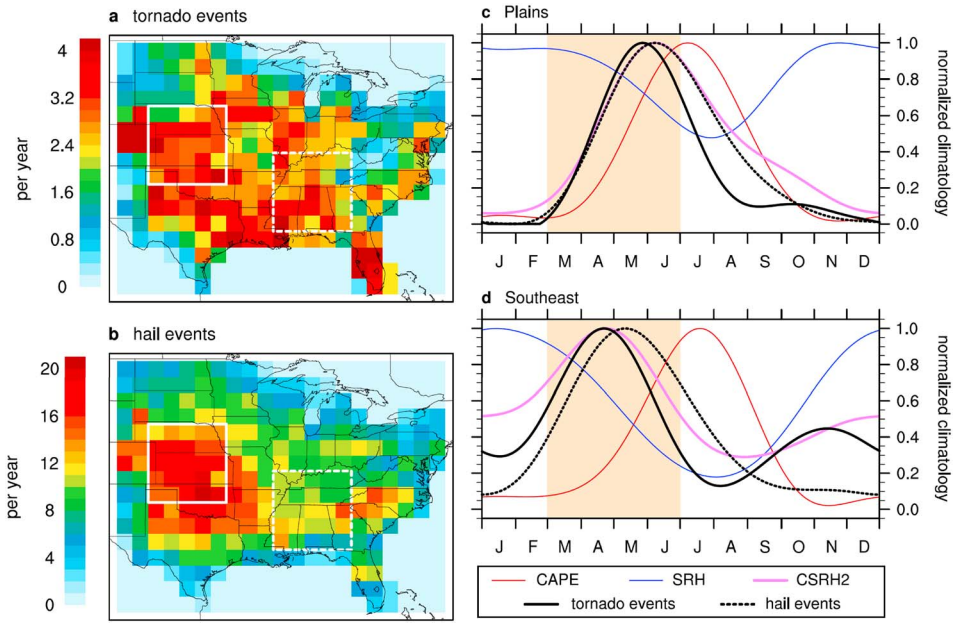

Figure 1. The climatological number of (a) tornado events and (b) hail events per year are shown, averaged over the years 1979–2015 for each 1.5° × 1.5° grid box. The Plains and the Southeast are delimited by solid white and dashed white lines, centered at (261°E, 39°N) and (273°E, 34.5°N), respectively. (c and d) Smoothed seasonal cycles of convective available potential energy (CAPE; red), storm relative helicity (SRH; blue), CSRH2 (violet), tornado events (solid black), and hail events (dashed black) are shown, computed over the (c) Plains and (d) Southeast. The season of interest, March–June, is shaded in light brown. The seasonal cycle for each variable has been normalized by its respective annual maximum. For the Plains, the annual maxima for CAPE, SRH, CSRH2, tornado events, and hail events are 871 J/kg, 131 m^2/s^2, 1.00 × 10^7 m^6/s^6, 0.710 events per day, and 3.11 events per day, respectively; for the Southeast, they are 868 J/kg, 142 m^2/s^2, 4.56 × 10^6 m^6/s^6, 0.413 events per day, and 1.68 events per day, respectively.

forecast sample. This process is repeated 1,000 times to create a distribution of random forecast samples for each combination of MJO phase and lead time. We assign three levels of significance to certain combinations of MJO phase and lead time if the observed forecast has a skill score that exceeds 80%, 90%, and 95% (alpha levels) of the skill scores found in the distribution of random forecast skill scores.

The statistical significance presented in section 4 for the composites is also assessed via a bootstrapping method with 1,000 random samples that account for autocorrelation in the observed data. Further details are provided in each figure's caption.

3. Climatology of Severe Weather Variables

Tornadoes and severe hail storms are common across the United States, generating thousands of storm reports annually (Schaefer & Edwards, 1999). In this study, we focus principally on the Plains and the Southeast, two regions heavily impacted by severe weather losses (NOAA/NCEI, 2018); however, we provide results summarizing other regions across the United States in our forthcoming presentations of Figures 3, 4, and 6. In Figure 1, we introduce the spatial and temporal characteristics of the severe weather variables relevant to our study. Figure 1a reveals that most locations east of the Rockies experience ~2 to 4 tornado events per year. In contrast, hail events (Figure 1b) show a distinct preference over the Plains (box delineated in solid white), with frequencies often greater than 12 events per year. Hail events are less common over the Southeast (box delineated in dashed white) where frequencies are generally less than 12 events per year. While some of the noise in these tornado and hail climatologies could be due to the finite duration of the time series we are considering (1979–2015), there are also well-documented, nonmeteorological heterogeneities in the data record (e.g., Agee & Childs, 2014; Allen & Tippett, 2015), which we discuss in Text S1.

Tornado and hail events over the Plains and Southeast are summed over their corresponding 7.5° × 7.5° regions (25 grid boxes), from which we derive their smoothed seasonal cycles (see section 2.4). Figures 1c

and 1d reveal that tornado and hail events (black and dashed black lines, respectively) peak during MAMJ (shaded in light brown) in both regions, with events peaking approximately 1 month earlier in the season over the Southeast. Severe thunderstorms are most common during MAMJ because the large-scale environmental conditions most favorable for their development—namely, instability, high vertical wind shear, and convective initiation mechanisms (e.g., drylines, frontal passages, and short wave troughs)—are most likely to be realized together at this time of year (Tippett et al., 2015). Initiation mechanisms are difficult to quantify (Tippett et al., 2015) and thus will only be analyzed from a large-scale perspective of how 500-hPa height anomalies promote surface-level patterns favorable to convective initiation and how these height anomalies are modified by the MJO. We focus more intensely on CAPE and SRH, common measures of instability and directional wind shear, respectively (e.g., Allen et al., 2015a; Barrett & Gensini, 2013; Barrett & Henley, 2015; Brooks et al., 2003; Gensini & Ashley, 2011; Tippett, 2014; Tippett et al., 2012, 2014, 2015). Also, we examine a combined environmental parameter, CSRH2, because it exhibits higher covariance with tornado and hail reports than either CAPE or SRH alone (Lu et al., 2015; Tippett et al., 2012, 2014). In fact, Figures 1c and 1d provide evidence that CSRH2 (violet line) serves as a reasonable proxy to tornado and hail events for both the Plains and the Southeast, as the peak in the seasonal cycle of CSRH2 is more aligned with them compared to either CAPE (red line) or SRH (blue line). It is certainly possible that combined environmental parameters other than CSRH2 have better empirical fits with tornado and hail events, particularly when location and time of year are considered (e.g., Allen et al., 2015a; Rasmussen & Blanchard, 1998; Tippett et al., 2014, 2015). However, an exhaustive examination of these environmental parameters is not the principal focus of our study. Rather, our findings involving CAPE, SRH, and CSRH2 are simply meant to lend support to our findings related to actual tornado and hail events.

4. Subseasonal Modulation by the MJO

Figure 2 displays composites of weekly averaged values of anomalous CAPE, SRH, and CSRH2 along with weekly summed values of anomalous tornado and hail events. Each composite is presented as a function of MJO phase and lead time for both the Plains and the Southeast. At zero lead times, we observe modulation of the severe weather variables by MJO phase that qualitatively agree with prior studies (Barrett & Gensini, 2013; Barrett & Henley, 2015; Thompson & Roundy, 2013). For example, as in Thompson and Roundy (2013), we observe at short lead times a higher frequency of tornado events when the MJO is in phase 2 in contrast to phase 8 when we observe lower frequencies (Figures 2d and 2i). However, what is novel here is the clear propagating signal of the anomalies through MJO phase and lead time space that extends to subseasonal lead times of 2–5 weeks—not only of the environmental parameters but of the tornado and hail events themselves. These anomalies often approach deviations of ~30% from their climatological March–July values. Moreover, the magnitudes of the anomalies generally do not weaken with lead time and in fact show signs of strengthening at lead times of 2–3 weeks. This behavior is consistent with the ~10–14 days that Rossby waves take to travel from the tropics and influence the United States (Sardeshmukh & Hoskins, 1988; Zhang, 2013). Also, the observed propagation through MJO phase and lead time space is consistent with the period of a typical MJO of ~30–60 days (Kiladis et al., 2014; Matthews, 2008; Wheeler & Hendon, 2004). For example, in Figure 2a, the highest values of anomalous CAPE reside in each MJO phase for ~5 days, transitioning from occurring immediately following phase 4 to ~20 days following phase 1.

We wish to note that we purposely do not show statistical significance in our presentation of Figure 2. Instead, we wish to emphasize the clear propagating signal through MJO phase and lead time space that extends through the composites rather than focus on the significance of any particular grid point. It can be reasonably surmised that these propagating signals do not happen by chance. Nevertheless, to see statistical significance, we reproduce Figure 2 in Figure S1. As expected, the largest anomalies along the propagating signals through MJO phase and lead time space are significant, particularly in the Plains (Figures S1a to S1e). While grid point by grid point significance is less over the Southeast, the propagating signals are still present, which lends confidence that there is a dynamical link to the MJO (e.g., SRH and tornado events in Figure S1g and S1i, respectively).

Returning to our discussion of Figure 2, we note that not only are the environmental parameters of CAPE, SRH, and CSRH2 modulated by the MJO at extended lead times, the actual tornado and hail events are as

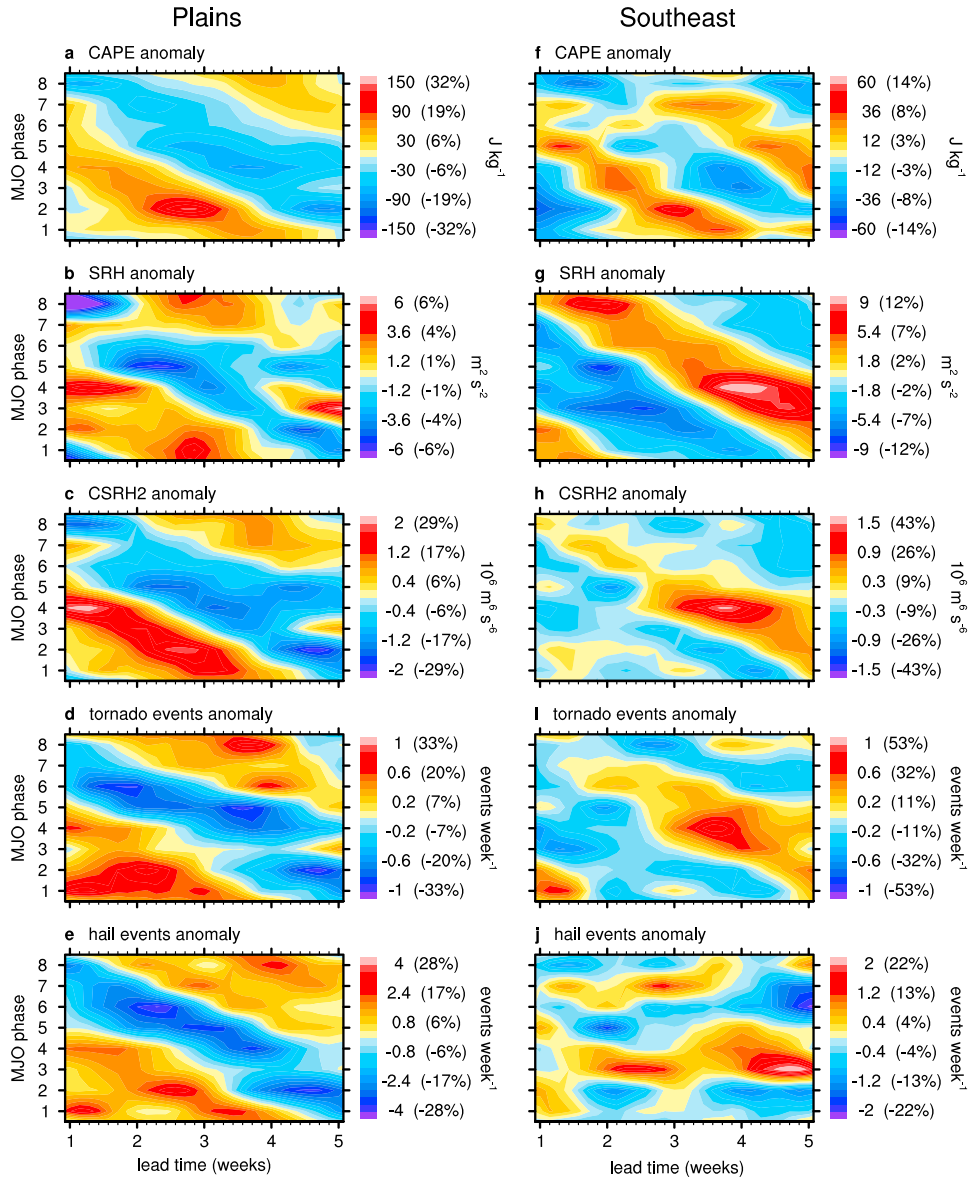

Figure 2. Weekly composites of anomalous (a and f) convective available potential energy (CAPE), (b and g) storm relative helicity (SRH), (c and h) CSRH2, (d and i) tornado events, and (e and j) hail events for the (a–e) Plains and (f–j) Southeast are plotted. For example, the maximum in SRH in (g) at a lead time of 4 weeks following phase 4 of the Madden-Julian Oscillation (MJO) represents the weekly averaged value of anomalous SRH for lead times spanning 22–28 days, while the maximum value in tornado events in (d) at a lead time of 2 weeks following phase 2 of the MJO represents the weekly summed value of anomalous tornado events for the lead times spanning 8–15 days. Percentages indicate a given anomaly's deviation from its March–July climatological value. Pattern means are removed before plotting. In Figure S1, we display Figure 2 with its statistical significance plotted and the plotting function's smoothing turned off.

well (Figures 2d, 2e, 2i, and 2j). In particular, the tornado and hail events in the Plains have propagating signals through MJO phase and lead time space entirely consistent with those of the aforementioned parameters. Pattern correlations calculated across MJO phase and lead time space between the composites of tornado events with those of CAPE, SRH, and CSRH2 in the Plains are 0.58, 0.59, and 0.72, respectively. For hail events, the values are 0.68, 0.54, and 0.73. Each value is significant at the 95% confidence level. While the pattern correlations in the Plains reveal that CSRH2 is a better proxy for tornado and hail events than CAPE or SRH alone, this is supported even more in the Southeast. There, tornado events have pattern correlations of −0.29, 0.68, and 0.76 with CAPE, SRH, and CSRH2, respectively.

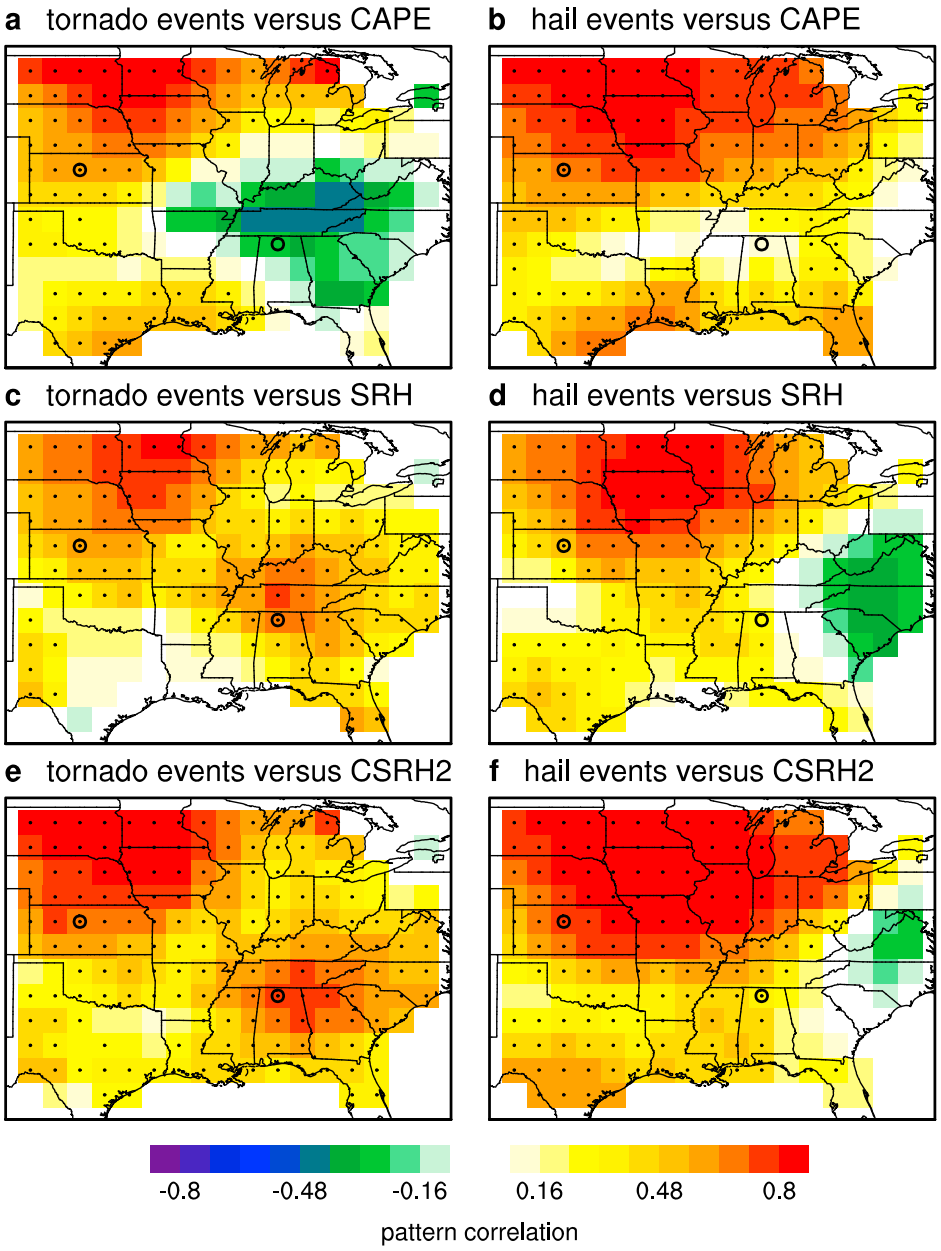

Figure 3. Centered pattern correlations that are calculated across 8 Madden-Julian Oscillation (MJO) phases and 31 lead times are shown for (a) tornado events versus convective available potential energy (CAPE), (c) tornado events versus storm relative helicity (SRH), (e) tornado events versus CSRH2, (b) hail events versus CAPE, (d) hail events versus SRH, and (f) hail events versus CSRH2. The open black circles highlight the pattern correlations discussed in the text for the Plains and the Southeast, as derived from the composites in Figure 2. The remaining values represent the pattern correlations between the composites that are calculated for each overlapping 7.5° × 7.5° region, centered every 1.5° in longitude from 258.0 to 282.0°E, and every 1.5° in latitude from 28.5 to 45.0°N. We only display values for regions whose central grid box overlaps the landmass of the United States. Statistical significance is assessed via a bootstrapping method that accounts for autocorrelation (see section 2.6). Each black dot indicates that a given pattern correlation exceeds 95% of 1,000 randomly generated pattern correlations. The random pattern correlations are generated by producing random composites of tornado and hail events (across MJO phase and lead time space) and then calculating their pattern correlations with the observed composites of CAPE, SRH, and CSRH2.

For hail events, the values are 0.13, 0.27, and 0.39. The pattern correlations involving CAPE are not significant at the 95% confidence level, but those involving CSRH2 are. As illustrated in Figure 3, the aforementioned pattern correlations associated with the Plains and Southeast regions (highlighted by

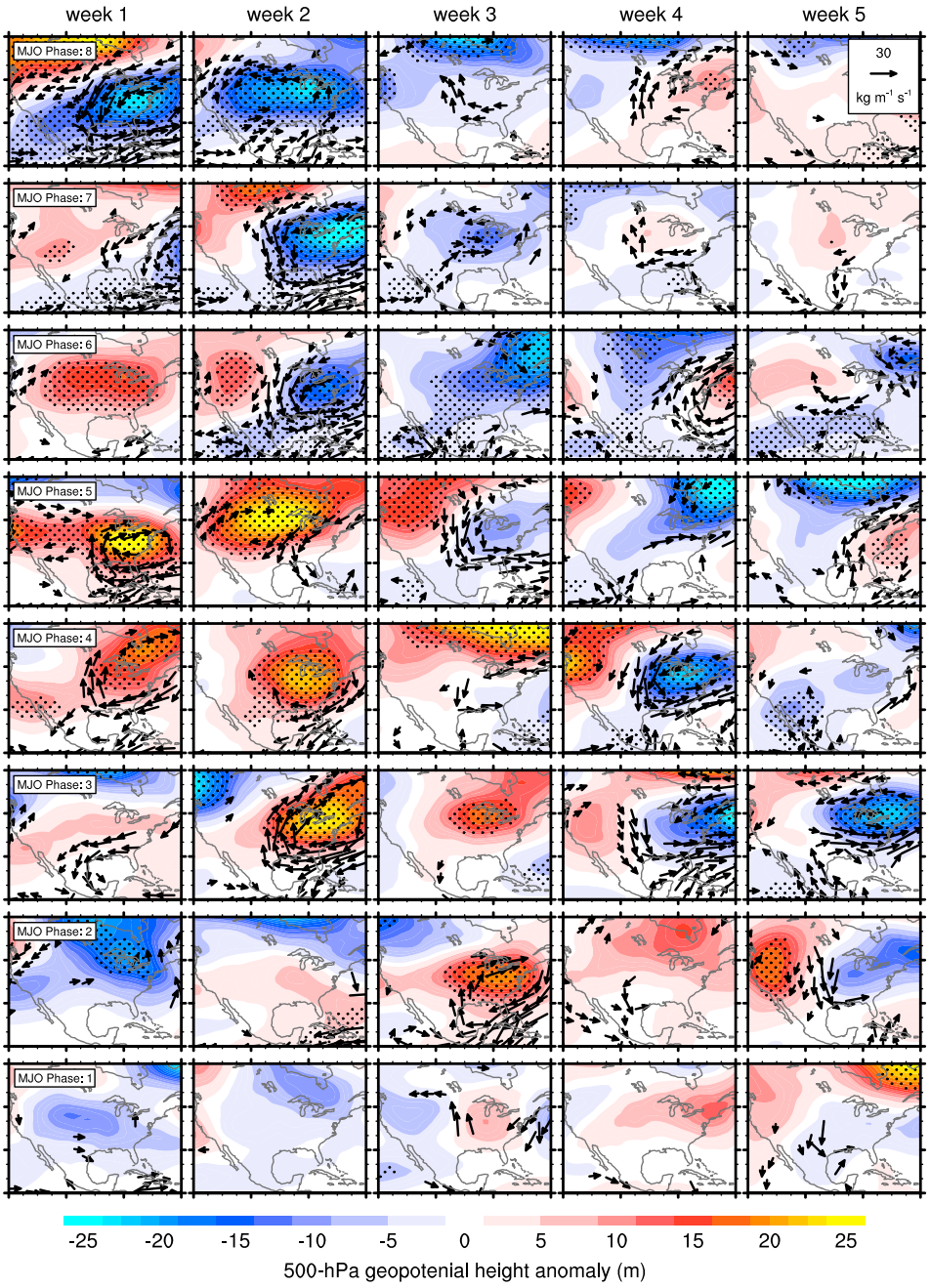

Figure 4. Composites of anomalous, weekly averaged 500-hPa heights (m) and vertically integrated vapor transport (IVT; $kg \cdot m^{-1} \cdot s^{-1}$) are shown. From top to bottom, the rows correspond to Madden-Julian Oscillation (MJO) phases 8 through 1, respectively. From left to right, the columns correspond to lead weeks 1 through 5, respectively. Each panel encompasses a longitudinal range of 235.0 to 295.0°E and a latitudinal range of 15.0 to 60.0°N. The black vectors depict anomalous IVT, where $IVT = \boldsymbol{i}\left(\frac{1}{g}\int_{1,000\ hPa}^{300\ hPa} uqdp\right) + \boldsymbol{j}\left(\frac{1}{g}\int_{1000\ hPa}^{300\ hPa} vqdp\right)$. Here u is zonal wind, v is meridional wind, q is specific humidity, dp is the difference between reanalysis pressure levels, and g is the acceleration of gravity; $\boldsymbol{i}$ and $\boldsymbol{j}$ represent the unit vectors in the zonal and meridional directions, respectively. Statistical significance is assessed via a bootstrapping method that accounts for autocorrelation (see section 2.6). The method produces a distribution of 1,000 random composites for each component of IVT and 500-hPa heights that vary according to MJO phase and lead week. Only composited anomalous IVT vectors with magnitudes exceeding 10 $kg \cdot m^{-1} \cdot s^{-1}$ and having either component statistically significant at the 95% confidence level are plotted. Stippling denotes where the 500-hPa heights anomalies are significant at the 95% confidence level. A two-tailed test is employed.

the black open circles that represent the centers of these 7.5° × 7.5° regions) are representative of the pattern correlations associated with their neighboring regions. These pattern correlations are derived from the composites (not shown) of overlapping 7.5° × 7.5° regions, centered every 1.5° in longitude from 258.0 to 282.0°E and every 1.5° in latitude from 28.5 to 45.0°N. This analysis illustrates the utility of a combined parameter, such as CSRH2, in diagnosing environments favorable to severe weather at subseasonal timescales, as the relative importance of CAPE and SRH differs by region and by season. For example, CAPE exhibits negative pattern correlations with tornado events for regions over the southeastern United States during MAMJ (Figure 3a) while SRH (Figure 3c) and CSRH2 (Figure 3e) have significantly positive pattern correlations during this period. Indeed, it has been shown that kinematic parameters such as SRH can be more useful as a severe weather discriminator than thermodynamic parameters, such as CAPE (Grams et al., 2012; Tippett et al., 2015). Furthermore, there exists a propensity for high-shear, low-CAPE severe weather environments in the Southeast, due in part to lower lapse rates, as compared to the Plains (Sherburn & Parker, 2014).

It is useful to examine how 500-hPa height anomalies vary by MJO phase and lead time (Figure 4) in order to physically explain the observed modulation of the environmental parameters of CAPE, SRH, and CSRH2. Moreover, an examination of 500-hPa height anomalies can also reveal some plausible convective initiation mechanisms. Because the MJO induces Rossby waves that propagate into the midlatitudes, it is capable of modulating the 500-hPa height patterns over the United States (Baggett et al., 2017; Henderson et al., 2016; Mundhenk et al., 2018; Sardeshmukh & Hoskins, 1988; Zhang, 2013). The composites in Figure 4 reveal that significant modulation of the 500-hPa heights, taking the form of anomalous troughs and ridges, exists for most MJO phases and lead weeks. In fact, upon closer inspection, these anomalous troughs and ridges propagate across MJO phase and lead week in a manner consistent with the approximately 30- to 60-day period of a typical MJO. For example, the anomalous ridge in the eastern United States that exists during the first week following phase 4 transitions to occur in the third week following phase 2. Similarly, the anomalous trough in the eastern United States that exists during the first week following phase 8 transitions to occurring in the fifth week following phase 3. The location of the troughs and ridges are physically important because they help explain the observed modulation of the severe weather variables displayed in Figure 2. At a basic level, a favorable height pattern in the Plains for severe weather consists of an anomalous ridge over the eastern United States paired with a trough to the west (e.g., during week 2 following phase 3 in Figure 4). Consistent with Figure 2a, this pattern enhances CAPE by inducing anomalous moisture transport out of the Gulf of Mexico (as indicated by the black vectors, which represent vertically integrated vapor transport). Also consistent with Figure 2b, this pattern provides support for convective initiation and organization as any short wave troughs or cold fronts that rotate through the trough can provide upper level divergence, synoptic-scale upward vertical motion, and vertical shear, as expected from quasi-geostrophic theory (Eady, 1949).

To conclude this section, we note that in some respects, it is surprising to see the modulation of 500-hPa heights and severe weather variables at such extended lead times across all MJO phases during MAMJ. Some prior studies have shown that the MJO's ability to generate Rossby waves is dependent on the phase of the MJO, that Rossby wave generation is most prominent during boreal winter, that these Rossby waves only exist for ~15 days, and that the teleconnections produced by these Rossby waves can vary at monthly timescales (e.g., Barrett & Henley, 2015; Cassou, 2008; Seo & Son, 2012). To reconcile these studies with our own, it is important to consider that the MJO has a typical propagation period of ~30–60 days. Therefore, if a particular phase of the MJO physically forces a teleconnection, then that same teleconnection may appear in our composites for other phases of the MJO without actually being forced by those phases. However, because the MJO typically exhibits a semicoherent progression through sequential phases (Matthews, 2008), the teleconnection will appear at different lead times in our composites—longer lead times for phases prior to the phase responsible for the forcing and shorter lead times for phases following the phase responsible for the forcing. Propagating teleconnections through MJO phase and lead time space are highlighted in our earlier discussions of Figures 2 and 4. Also, while most studies have focused on the MJO's influence during boreal winter, this does not preclude the MJO having a substantial influence during MAMJ. While our study and others (Barrett & Gensini, 2013; Barrett & Henley, 2015; Thompson & Roundy, 2013) demonstrate a statistical connection between the MJO and severe weather over the United States during MAMJ, studies with a more dynamical focus, such as idealized model simulations, would be worthwhile.

5. Skillful Subseasonal Forecasts Using the MJO

The composites in Figure 2 offer compelling evidence that the MJO modulates severe weather activity over the Plains and Southeast at subseasonal lead times. Therefore, a natural question to ask is whether the MJO is in fact a source of predictive skill—in other words, can we skillfully forecast severe weather activity at subseasonal lead times with knowledge of the current MJO state? To answer this question, we employ the empirical prediction model (explained in detail in section 2.5) to issue forecasts for consecutive, overlapping weeks with forecast leads of 1–29 days after the day the forecast is issued. It is important to emphasize here that forecasts are not being made to predict the occurrence of a specific severe thunderstorm on a particular day at a precise location. Rather, the forecasts are issued for above or below normal activity in broad 7.5° × 7.5° regions over weekly time scales.

Figure 5 presents the skill scores of the empirical prediction model for forecasts of CAPE, SRH, CSRH2, tornado events, and hail events for both the Plains and the Southeast. The shaded regions indicate where the model has positive skill and thus is more skillful than an equal-chances, random forecast. Warm and cool colors denote when above or below normal activity is forecast, respectively. In a manner consistent with the composites (Figure 2), positive skill scores propagate through MJO phase and lead time space for each environmental parameter in both the Plains and the Southeast (Figures 5a–5c and 5f–5h). Moreover, for the Plains, we see significantly positive, propagating skill scores for actual tornado and hail events (Figures 5d and 5e). Generally, the highest skill scores are collocated with the highest anomalies in the composites (compare Figures 2 and 5). Some of these high skill scores have values approaching 33, which implies a 2:1 ratio of correct to incorrect forecasts, a significant improvement over an equal-chances, random forecast. Most importantly, these significantly positive skill scores extend to forecast lead times of 2–5 weeks, well into subseasonal timescales. These forecast lead times for environmental parameters favorable to severe weather activity represent a significant improvement over the midlatitude predictability barrier of ~14 days that currently exists in state-of-the-art, numerical weather models (Baggett et al., 2017; Carbin et al., 2016; Vitart, 2017). Furthermore, the forecast lead times on display for actual tornado and hail events in the Plains offer an opportunity to extend short-term, daily outlooks (such as those issued by SPC) to subseasonal, weekly outlooks.

We test the robustness of our prediction model by performing a leave-three-years-out cross-validation approach. Overall we find our results to be qualitatively insensitive to using a leave-three-years-out versus a leave-one-year-out cross-validation approach (compare Figures 5 and S2). Moreover, our results are qualitatively insensitive to the choice of MJO index (compare Figures 2 and 5 to Figures S3 and S4, respectively), although skill scores are generally higher using the OMI rather than the RMM index. We hypothesize that this difference in skill scores results from the OMI being more directly analogous to OLR (and by extension, tropical convection, Rossby wave source dynamics, and midlatitude teleconnections) than the RMM, which also incorporates equatorial zonal winds (Kiladis et al., 2014; Sardeshmukh & Hoskins, 1988; Wheeler & Hendon, 2004). Testing of this hypothesis is beyond the scope of our study.

The combinations of MJO phase and forecast lead time that have significantly positive skill scores should be considered *forecasts of opportunity* because there are many other combinations that have very small positive or negative skill scores (white shading in Figure 5). Thus, a forecaster would need to be opportunistic in issuing forecasts when they have a higher probability of success. Moreover, the combinations of MJO phase and forecast lead time that have significantly positive skill scores vary by region. This is particularly true when comparing the relatively high skill scores of the forecasts generated for tornado and hail events in the Plains to those in the Southeast, where little skill is observed (compare Figures 5d and 5e to Figures 5i and 5j, respectively). In fact, when the skill scores are averaged over MJO phase and lead time space for each overlapping 7.5° × 7.5° region (Figure 6), it becomes quickly apparent that regions located in the Plains consistently exhibit higher average skill scores for each severe weather variable than other regions, while regions located in the South have relatively lower average skill scores for each variable except SRH (Figure 6b). Interestingly, with respect to SRH, there is a band of lower average skill scores running from the Central Plains through the Ohio River Valley, suggesting that the underlying variability of the jet stream for a given MJO phase has a more negative impact on predictability there than elsewhere. While understanding the root cause of these different average skill scores across regions is beyond the current scope of this study, it is important to emphasize that forecasts of opportunity exist in most regions and that these forecasts of opportunity vary by MJO phase and forecast lead time. For example, if a forecaster

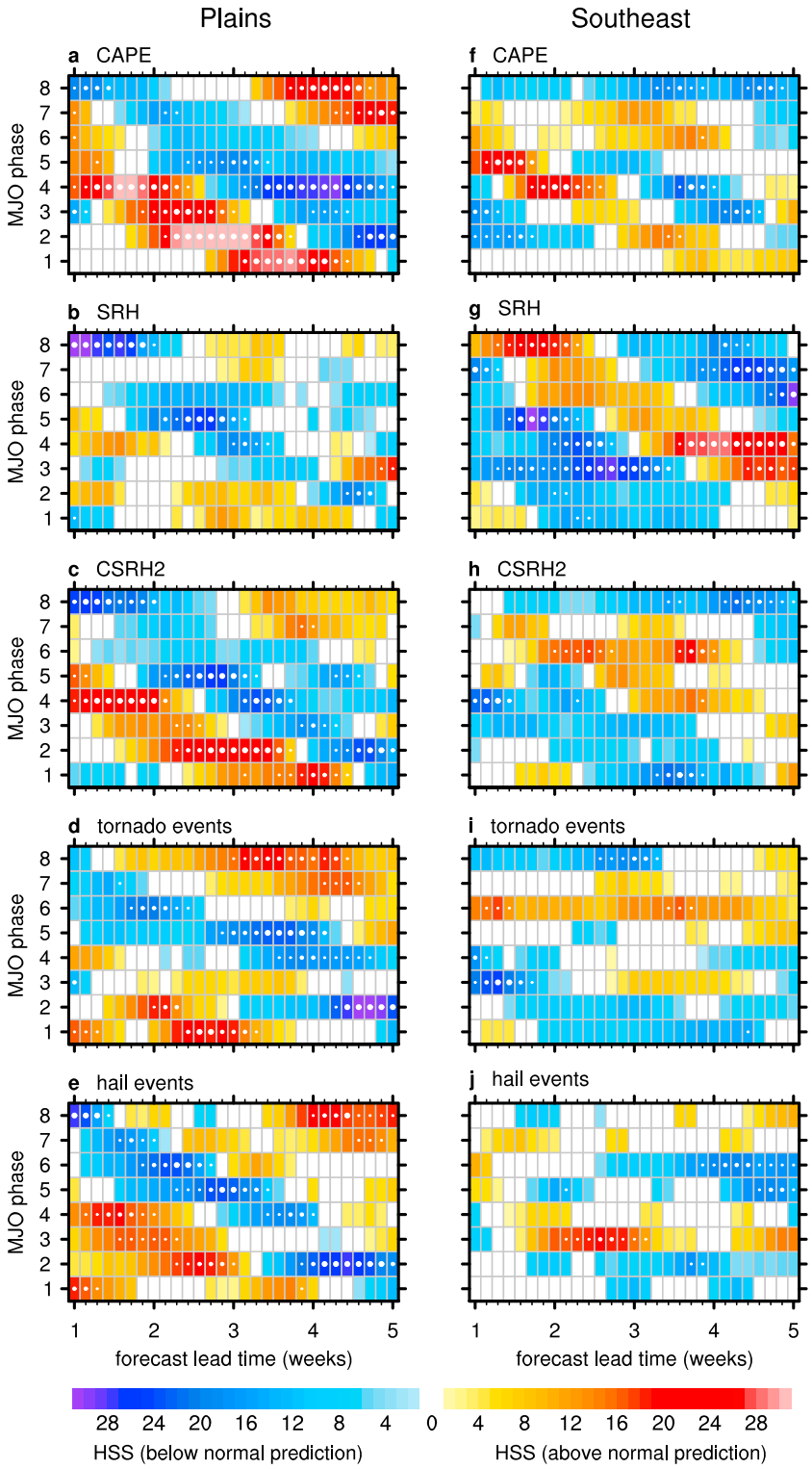

Figure 5. Heidke skill scores of the empirical prediction model are shown for (a and f) convective available potential energy (CAPE), (b and g) storm relative helicity (SRH), (c and h) CSRH2, (d and i) tornado events, and (e and j) hail events for the (a–e) Plains and (f–j) Southeast. Regions shaded in color have positive skill scores; regions shaded in white have negative skill scores. Warm and cool colors indicate predictions of above and below normal activity, respectively. Statistical significance is conveyed by small, medium, and large white dots for predictions that are more skillful than 80%, 90%, and 95%, respectively, of 1,000 random forecast samples generated by a bootstrapping technique that accounts for autocorrelation (see section 2.6).

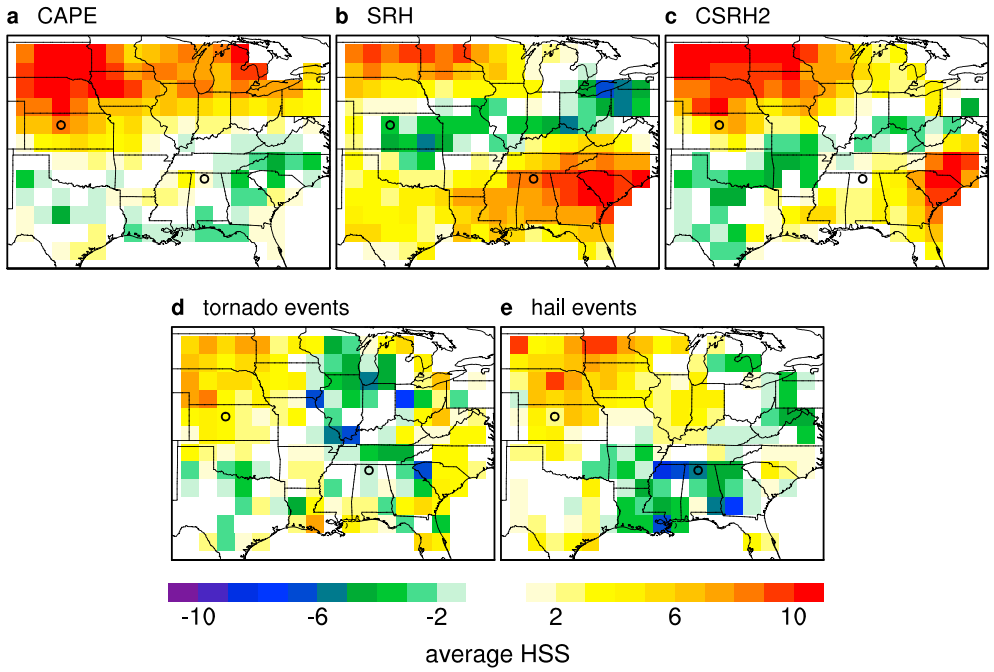

Figure 6. Heidke skill scores that are averaged across eight Madden-Julian Oscillation (MJO) phases and 29 lead times for the empirical prediction of (a) convective available potential energy (CAPE), (b) storm relative helicity (SRH), (c) CSRH2, (d) tornado events, and (e) hail events are shown. The open black circles represent the average skill scores for the Plains and the Southeast, as derived from Figure 5. The remaining values represent the averages for each overlapping 7.5° × 7.5° region, centered every 1.5° in longitude from 258.0 to 282.0°E and every 1.5° in latitude from 28.5 to 45.0°N. We only display values for regions whose central grid box overlap the landmass of the United States. Before being averaged, the individual skill scores are weighted by the sample size of its corresponding MJO phase (see Table S1).

wishes to issue guidance for tornado activity at a lead time of 4 weeks (Figure 5d), then he or she should have confidence in above normal activity in the Plains if the MJO was currently in phases 7 or 8.

6. Conclusion and Discussion

Using only the current phase of an active MJO as a predictor, we have constructed a simple two-class empirical model that provides skillful subseasonal forecasts for several large-scale environmental parameters associated with severe weather activity, namely, CAPE, SRH, and CSRH2. Moreover, we have demonstrated skillful forecasts of actual tornado and hail events in certain regions, such as the Plains, with lead times extending out to 5 weeks. While the principal question we set out to answer in this study revolved around the ability of the MJO to serve as a source of predictive skill, the simplicity of the two-class empirical model we developed lends opportunity to the addition of more predictors and additional classes that could lead to its improvement. Some potential predictors that operate on subseasonal and longer time scales include ENSO (Allen et al., 2015b; Childs et al., 2018; Cook et al., 2017; Lepore et al., 2017), the Global Wind Oscillation (Gensini & Allen, 2018; Gensini & Marinaro, 2016; Moore, 2017), Gulf of Mexico sea surface temperatures (Molina et al., 2016), antecedent drought conditions (Shepherd et al., 2009), the quasi-biennial oscillation (Baggett et al., 2017; Mundhenk et al., 2018; Son et al., 2017), the Arctic oscillation (Childs et al., 2018), and decadal-scale trends (Diffenbaugh et al., 2013; Tippett, 2014). ENSO has been shown to be a skillful predictor of severe weather activity at seasonal time scales (Allen et al., 2015b; Lepore et al., 2017). Thus, an empirical prediction model that uses both ENSO and the MJO as predictors (e.g., Slade & Maloney, 2013) may provide additional skill by capturing the subseasonal modulation of severe weather activity by the MJO juxtaposed onto the interannual modulation by ENSO. With respect to the quasi-biennial oscillation, recent work has shown that it impacts the amplitude of the MJO and therefore the MJO's impact on weather downstream (Baggett et al., 2017; Mundhenk et al., 2018; Son et al., 2017). Further, the Arctic oscillation, whose influence is most realized during winter and spring over the eastern United States, may be particularly useful in

improving skill scores in the Southeast (Childs et al., 2018), where severe weather peaks earlier in the year (Figures 1c and 1d).

Numerical weather models also offer hope in improving predictions of environmental parameters favorable to severe weather activity. Individual model runs of the Climate Forecast System, version 2 (CFSv2), generally show skill in predicting such environments with lead times of ~7 days (Carbin et al., 2016). However, Carbin et al. (2016) demonstrated that the possibility exists to extend these skillful lead times by several weeks through a lagged ensemble approach whereby consecutive model runs serve as an ensemble prediction for the same forecast verification date. Development of an empirical prediction model that uses both the lagged ensemble approach and the MJO as predictors could prove a useful venture to that end. With respect to the MJO, numerical models are increasingly skillful at predicting its propagation along the equator, with skillful lead times of 4–5 weeks realized by the ECMWF model (Kim et al., 2016; Vitart, 2017). It is conceivable that the skillful lead times of an empirical model can be extended by initializing it with a numerical model's forecasted state of the MJO. Regardless of how our empirical model's skill is eventually improved, our results show that knowledge of the MJO is an important source of predictability *and* prediction skill of tornado and severe hail events for certain weeks and regions at lead times of 2–5 weeks. While it remains to be seen if the forewarning provided by the MJO is actionable in real time by emergency managers and stakeholders to protect lives and property, these results nonetheless represent an important scientific advancement in our understanding of an important source of subseasonal predictability of severe weather.

Acknowledgments
This research has been conducted as part of the NOAA MAPP S2S Prediction Task Force and supported by NOAA grant NA16OAR4310064. Additional support was received from NSF Climate and Large-scale Dynamics Program grant AGS-1441916, NWS grant NA16NWS4680022, NSF Graduate Research Fellowship Program grant DGE-1321845, NSF REU Site in Climate Science at CSU grant AGS-1461270, and a subaward under the FIRO project at CW3. We thank Michael K. Tippett for fostering dialogue and five anonymous reviewers who have all helped to improve the manuscript. All coding was performed in the National Center for Atmospheric Research Command Language (NCL) version V.6.4.0, Python V.2.7.12, the Sounding and Hodograph Analysis and Research Program in Python (SHARPpy) V.1.3.0, and Matlab V. R2015b. Access information to all data repositories is provided in Text S2.

References

Agee, E., & Childs, S. (2014). Adjustments in tornado counts, F-scale intensity, and path width for assessing significant tornado destruction. *Journal of Applied Meteorology and Climatology*, *53*(6), 1494–1505. https://doi.org/10.1175/jamc-d-13-0235.1

Allen, J. T., & Tippett, M. K. (2015). The characteristics of United States hail reports: 1955-2014. *Electronic Journal of Severe Storms Meteorology*, *10*, 1–31.

Allen, J. T., Tippett, M. K., & Sobel, A. H. (2015a). An empirical model relating U.S. monthly hail occurrence to large-scale meteorological environment. *Journal of Advances in Modeling Earth Systems*, *7*, 226–243. https://doi.org/10.1002/2014ms000397

Allen, J. T., Tippett, M. K., & Sobel, A. H. (2015b). Influence of the El Nino/Southern Oscillation on tornado and hail frequency in the United States. *Nature Geoscience*, *8*(4), 278–283. https://doi.org/10.1038/Ngeo2385

Allen, J. T., Tippett, M. K., Sobel, A. H., & Lepore, C. (2016). Understanding the drivers of variability in severe convection: Bringing together the scientific and insurance communities. *Bulletin of the American Meteorological Society*, *97*(11), ES221–ES223. https://doi.org/10.1175/bams-d-16-0208.1

Baggett, C. F., Barnes, E. A., Maloney, E. D., & Mundhenk, B. D. (2017). Advancing atmospheric river forecasts into subseasonal-to-seasonal timescales. *Geophysical Research Letters*, *44*, 7528–7536. https://doi.org/10.1002/2017gl074434

Barrett, B. S., & Gensini, V. A. (2013). Variability of central United States April-May tornado day likelihood by phase of the Madden-Julian Oscillation. *Geophysical Research Letters*, *40*, 2790–2795. https://doi.org/10.1002/grl.50522

Barrett, B. S., & Henley, B. N. (2015). Intraseasonal variability of hail in the contiguous United States: Relationship to the Madden-Julian Oscillation. *Monthly Weather Review*, *143*(4), 1086–1103. https://doi.org/10.1175/Mwr-D-14-00257.1

Blumberg, W. G., Halbert, K. T., Supinie, T. A., Marsh, P. T., Thompson, R. L., & Hart, J. A. (2017). SHARPpy: An open-source sounding analysis toolkit for the atmospheric sciences. *Bulletin of the American Meteorological Society*, *98*(8), 1625–1636. https://doi.org/10.1175/bams-d-15-00309.1

Brooks, H. E., Lee, J. W., & Craven, J. P. (2003). The spatial distribution of severe thunderstorm and tornado environments from global reanalysis data. *Atmospheric Research*, *67-68*, 73–94. https://doi.org/10.1016/s0169-8095(03)00045-0

Bunkers, M. J., Klimowski, B. A., Zeitler, J. W., Thompson, R. L., & Weisman, M. L. (2000). Predicting supercell motion using a new hodograph technique. *Weather and Forecasting*, *15*(1), 61–79. https://doi.org/10.1175/1520-0434(2000)015<0061:PSMUAN>2.0.CO;2

Carbin, G. W., Tippett, M. K., Lillo, S. P., & Brooks, H. E. (2016). Visualizing long-range severe thunderstorm environment guidance from CFSv2. *Bulletin of the American Meteorological Society*, *97*(6), 1021–1031. https://doi.org/10.1175/bams-d-14-00136.1

Cassou, C. (2008). Intraseaonal interaction between the Madden-Julian Oscillation and the North Atlantic Oscillation. *Nature*, *455*(7212), 523–527. https://doi.org/10.1038/nature07286

Childs, S. J., Schumacher, R. S., & Allen, J. T. (2018). Cold-season tornadoes: Climatological and meteorological insights. *Weather and Forecasting*, *33*(3), 671–691. https://doi.org/10.1175/waf-d-17-0120.1

Cook, A. R., Leslie, L. M., Parsons, D. B., & Schaefer, J. T. (2017). The impact of El Niño–Southern Oscillation (ENSO) on winter and early spring U.S. tornado outbreaks. *Journal of Applied Meteorology and Climatology*, *56*(9), 2455–2478. https://doi.org/10.1175/jamc-d-16-0249.1

Dee, D. P., Uppala, S. M., Simmons, A. J., Berrisford, P., Poli, P., Kobayashi, S., Andrae, U., et al. (2011). The ERA-Interim reanalysis: Configuration and performance of the data assimilation system. *Quarterly Journal of the Royal Meteorological Society*, *137*(656), 553–597. https://doi.org/10.1002/qj.828

Diffenbaugh, N. S., Scherer, M., & Trapp, R. J. (2013). Robust increases in severe thunderstorm environments in response to greenhouse forcing. *Proceedings of the National Academy of Sciences of the United States of America*, *110*(41), 16,361–16,366. https://doi.org/10.1073/pnas.1307758110

Eady, E. T. (1949). Long waves and cyclone waves. *Tellus*, *1*(3), 33–52. https://doi.org/10.1111/j.2153-3490.1949.tb01265.x

Gensini, V. A., & Allen, J. T. (2018). United States hail frequency and the global wind oscillation. *Geophysical Research Letters*, *45*, 1611–1620. https://doi.org/10.1002/2017gl076822

Gensini, V. A., & Ashley, W. S. (2011). Climatology of potentially severe convective environments from North American regional reanalysis. *Electronic Journal of Severe Storms Meteorology*, *6*(8), 1–40.

Gensini, V. A., & Marinaro, A. (2016). Tornado frequency in the United States related to global relative angular momentum. *Monthly Weather Review*, *144*(2), 801–810. https://doi.org/10.1175/mwr-d-15-0289.1

Grams, J. S., Thompson, R. L., Snively, D. V., Prentice, J. A., Hodges, G. M., & Reames, L. J. (2012). A climatology and comparison of parameters for significant tornado events in the United States. *Weather and Forecasting*, *27*(1), 106–123. https://doi.org/10.1175/waf-d-11-00008.1

Gunturi, P., & Tippett, M. K. (2017). Impact of ENSO on U.S. tornado and hail frequencies. Managing Severe Thunderstorm Risk, Technical Report, WillisRe.

Henderson, S. A., Maloney, E. D., & Barnes, E. A. (2016). The influence of the Madden-Julian Oscillation on Northern Hemisphere winter blocking. *Journal of Climate*, *29*(12), 4597–4616. https://doi.org/10.1175/Jcli-D-15-0502.1

Herman, G. R., Nielsen, E. R., & Schumacher, R. S. (2017). Probabilistic verification of Storm Prediction Center convective outlooks. *Weather and Forecasting*, *33*(1), 161–184. https://doi.org/10.1175/waf-d-17-0104.1

Johnson, N. C., Collins, D. C., Feldstein, S. B., L'Heureux, M. L., & Riddle, E. E. (2014). Skillful wintertime North American temperature forecasts out to 4 weeks based on the state of ENSO and the MJO*. *Weather and Forecasting*, *29*(1), 23–38. https://doi.org/10.1175/waf-d-13-00102.1

Kiladis, G. N., Dias, J., Straub, K. H., Wheeler, M. C., Tulich, S. N., Kikuchi, K., et al. (2014). A comparison of OLR and circulation-based indices for tracking the MJO. *Monthly Weather Review*, *142*(5), 1697–1715. https://doi.org/10.1175/Mwr-D-13-00301.1

Kim, H. M., Kim, D., Vitart, F., Toma, V. E., Kug, J. S., & Webster, P. J. (2016). MJO propagation across the maritime continent in the ECMWF Ensemble Prediction System. *Journal of Climate*, *29*(11), 3973–3988. https://doi.org/10.1175/Jcli-D-15-0862.1

Lepore, C., Tippett, M. K., & Allen, J. T. (2017). ENSO-based probabilistic forecasts of March-May U.S. tornado and hail activity. *Geophysical Research Letters*, *44*, 9093–9101. https://doi.org/10.1002/2017gl074781

Lu, M., Tippett, M. K., & Lall, U. (2015). Changes in the seasonality of tornado and favorable genesis conditions in the central United States. *Geophysical Research Letters*, *42*, 4224–4231. https://doi.org/10.1002/2015gl063968

Matthews, A. J. (2008). Primary and successive events in the Madden–Julian Oscillation. *Quarterly Journal of the Royal Meteorological Society*, *134*(631), 439–453. https://doi.org/10.1002/qj.224

McDonald, J. R., & Mehta, K. C. (2006). A recommendation for an Enhanced Fujita Scale (EF-Scale). Technical Report, Texas Tech University: Wind Science and Engineering Center.

Molina, M. J., Timmer, R. P., & Allen, J. T. (2016). Importance of the Gulf of Mexico as a climate driver for U.S. severe thunderstorm activity. *Geophysical Research Letters*, *43*, 12,295–12,304. https://doi.org/10.1002/2016gl071603

Moore, T. W. (2017). Annual and seasonal tornado activity in the United States and the global wind oscillation. *Climate Dynamics*, *50*(11–12), 4323–4334. https://doi.org/10.1007/s00382-017-3877-5

Mundhenk, B. D., Barnes, E. A., Maloney, E. D., & Baggett, C. F. (2018). Skillful empirical subseasonal prediction of landfalling atmospheric river activity using the Madden–Julian oscillation and quasi-biennial oscillation. *npj Climate and Atmospheric Science*, *1*(1), 1–7. https://doi.org/10.1038/s41612-017-0008-2

NOAA National Centers for Environmental Information (NCEI) (2018). U.S. billion-dollar weather and climate disasters. Retrieved from https://www.ncdc.noaa.gov/billions/

NOAA Storm Prediction Center (SPC) (2018). SPC Products. Retrieved from https://www.spc.noaa.gov/misc/about.html

Rasmussen, E. N., & Blanchard, D. O. (1998). A baseline climatology of sounding-derived supercell and tornado forecast parameters. *Weather and Forecasting*, *13*(4), 1148–1164. https://doi.org/10.1175/1520-0434(1998)013<1148:ABCOSD>2.0.CO;2

Sardeshmukh, P. D., & Hoskins, B. J. (1988). The generation of global rotational flow by steady idealized tropical divergence. *Journal of the Atmospheric Sciences*, *45*(7), 1228–1251. https://doi.org/10.1175/1520-0469(1988)045<1228:TGOGRF>2.0.CO;2

Schaefer, J. T., & Edwards, R. (1999). The SPC Tornado/Severe Thunderstorm Database. In Preprints, 11th Conference of Applied Meteorology. (pp. 215–220). Dallas TX: American Meteorological Society.

Seo, K. H., & Son, S. W. (2012). The global atmospheric circulation response to diabatic heating associated with the Madden-Julian Oscillation during northern winter. *Journal of the Atmopsheric Sciences*, *69*(1), 79–96. https://doi.org/10.1175/2011jas3686.1

Shepherd, M., Niyogi, D., & Mote, T. L. (2009). A seasonal-scale climatological analysis correlating spring tornadic activity with antecedent fall–winter drought in the southeastern United States. *Environmental Research Letters*, *4*(2), 1–7. https://doi.org/10.1088/1748-9326/4/2/024012

Sherburn, K. D., & Parker, M. D. (2014). Climatology and ingredients of significant severe convection in high-shear, low-CAPE environments. *Weather and Forecasting*, *29*(4), 854–877. https://doi.org/10.1175/waf-d-13-00041.1

Simmons, K., & Sutter, D. (2011). *Economic and societal impacts of tornadoes*. Boston: American Meteorological Society. https://doi.org/10.1007/978-1-935704-02-7

Slade, S. A., & Maloney, E. D. (2013). An intraseasonal prediction model of Atlantic and East Pacific tropical cyclone genesis. *Monthly Weather Review*, *141*(6), 1925–1942. https://doi.org/10.1175/mwr-d-12-00268.1

Smith, A. B., & Matthews, J. L. (2015). Quantifying uncertainty and variable sensitivity within the US billion-dollar weather and climate disaster cost estimates. *Natural Hazards*, *77*(3), 1829–1851. https://doi.org/10.1007/s11069-015-1678-x

Son, S. W., Lim, Y., Yoo, C., Hendon, H. H., & Kim, J. (2017). Stratospheric control of the Madden-Julian Oscillation. *Journal of Climate*, *30*(6), 1909–1922. https://doi.org/10.1175/Jcli-D-16-0620.1

Thompson, D. B., & Roundy, P. E. (2013). The relationship between the Madden-Julian Oscillation and US violent tornado outbreaks in the spring. *Monthly Weather Review*, *141*(6), 2087–2095. https://doi.org/10.1175/Mwr-D-12-00173.1

Tippett, M. K. (2014). Changing volatility of U.S. annual tornado reports. *Geophysical Research Letters*, *41*, 6956–6961. https://doi.org/10.1002/2014gl061347

Tippett, M. K., Allen, J. T., Gensini, V. A., & Brooks, H. E. (2015). Climate and hazardous convective weather. *Current Climate Change Reports*, *1*(2), 60–73. https://doi.org/10.1007/s40641-015-0006-6

Tippett, M. K., Sobel, A. H., & Camargo, S. J. (2012). Association of U.S. tornado occurrence with monthly environmental parameters. *Geophysical Research Letters*, *39*, L02801. https://doi.org/10.1029/2011GL050368

Tippett, M. K., Sobel, A. H., Camargo, S. J., & Allen, J. T. (2014). An empirical relation between U.S. tornado activity and monthly environmental parameters. *Journal of Climate*, *27*(8), 2983–2999. https://doi.org/10.1175/jcli-d-13-00345.1

Vitart, F. (2017). Madden-Julian Oscillation prediction and teleconnections in the S2S Database. *Quarterly Journal of the Royal Meteorological Society*, *143*(706), 2210–2220. https://doi.org/10.1002/qj.3079

Wheeler, M. C., & Hendon, H. H. (2004). An all-season real-time multivariate MJO index: Development of an index for monitoring and prediction. *Monthly Weather Review*, *132*(8), 1917–1932. https://doi.org/10.1175/1520-0493(2004)132<1917:AARMMI>2.0.CO;2

Wilks, D. S. (2006). *Statistical methods in the atmospheric sciences*, *Int. Geophys. Ser.* (2nd ed., Vol. 91). Burlington: Academic Press.

Zhang, C. (2013). Madden–Julian Oscillation: Bridging weather and climate. *Bulletin of the American Meteorological Society*, *94*(12), 1849–1870. https://doi.org/10.1175/BAMS-D-12-00026.1